



1 **Evidence of ketene emissions from petrochemical industries and implications for**
2 **ozone production potential**

3 Chinmoy Sarkar^{1,a,*}, Gracie Wong¹, Anne Mielnik¹, Alex B. Guenther¹, Taehyoung Lee², Taehyun
4 Park², Jihee Ban², Seokwon Kang², Jin-Soo Park³, Joonyoung Ahn³, Danbi Kim³, Hyunjae Kim³,
5 Jinsoo Choi³, Beom-Keon Seo⁴, Jong-Ho Kim⁴, Jeong-Ho Kim⁵, Soo Bog Park⁴, Saewung Kim^{1,*}

6 ¹Department of Earth System Science, University of California Irvine, 92697, California, USA

7 ²Department of Environmental Science, Hankuk University of Foreign Studies, Yongin 17035,
8 South Korea

9 ³ National Institute of Environmental Research, Inchoen 22689, South Korea

10 ⁴Institute of Environmental Research, Hanseo University, Seosan-si, South Korea

11 ⁵APM Engineering Co. Ltd., Seoul, South Korea

12 ^anow at: Air Quality Research Center, University of California Davis, One Shields Avenue, Davis,
13 CA 95616, USA

14 *Correspondence to: Chinmoy Sarkar (chinmoysarkar8@gmail.com) and Saewung Kim
15 (saewung.kim@uci.edu)

16

17

18

19

20

21

22

23

24

25

26

27

28



29 **Abstract**

30 Ketene, a rarely measured reactive VOC, was quantified in the emission plumes from Daesan
31 petrochemical facility in South Korea using airborne PTR-TOF-MS measurements. Ketene mixing
32 ratios as high as $\sim 40 - 50$ ppb were observed in the emission plumes. Emission rates of ketene
33 from the facility were estimated using a horizontal advective flux approach and ranged from $84 -$
34 316 kg h^{-1} . These emission rates were compared to the emission rates of major VOCs such as
35 benzene, toluene, and acetaldehyde. Significant correlations ($r^2 > 0.7$) of ketene with methanol,
36 acetaldehyde, benzene, and toluene were observed for the peak emissions, indicating commonality
37 of emission sources. The calculated average ketene OH reactivity for the emission plumes over
38 Daesan ranged from $3.33 - 7.75 \text{ s}^{-1}$, indicating the importance of the quantification of ketene to
39 address missing OH reactivity in the polluted environment. The calculated average O_3 production
40 potential for ketene ranged from $2.98 - 6.91 \text{ ppb h}^{-1}$. Our study suggests that ketene has the
41 potential to significantly influence local photochemistry and therefore, further studies focusing on
42 the photooxidation and atmospheric fate of ketene through chamber studies is required to improve
43 our current understanding of VOC OH reactivity and hence, tropospheric O_3 production.

44 **1. Introduction**

45 Reactive volatile organic compounds (VOCs) can have atmospheric lifetimes ranging from
46 minutes to days (Atkinson, 2000) and have significant influence on regional air quality as they
47 participate in atmospheric chemical reactions that leads to the formation of secondary pollutants
48 such as tropospheric ozone (O_3) and secondary organic aerosol (SOA). Both tropospheric O_3 and
49 SOA are important from the standpoint of air quality and human health and have impact on the
50 radiative forcing of the atmosphere (IPCC, 2013). In addition, through chemical reactions with the
51 hydroxyl radicals (major oxidant of the atmosphere; Lelieveld et al. (2004)), photodissociation and
52 radical recycling reactions, VOCs strongly influence the HO_x (OH, HO_2) radical budget that
53 controls the removal rates of gaseous pollutants from the atmosphere, including most greenhouse
54 gases (such as CH_4).

55 Ketene (ethenone; CAS: 674-82-8; $\text{H}_2\text{C}=\text{C}=\text{O}$) is a highly reactive oxygenated VOC. Recent
56 studies have revealed that gaseous ketene has very high pulmonary toxicity and can be lethal at
57 high concentrations (Wu and O'Shea, 2020). Ketene is formed due to pyrolysis reactions of
58 furfural derivatives and furans emitted during thermal cracking of cellulose and lignin in biomass
59 material (Kahan et al., 2013). Ozonolysis of propene and oxidation of heterocyclic oxepin
60 (benzene oxide) also produce ketene in the atmosphere (Klotz et al., 1997; McNelis et al., 1975).
61 Due to the presence of both double bond and carbonyl functional groups, ketene is highly reactive
62 and can play a significant role in ambient OH reactivity and hence OH recycling processes
63 (Lelieveld et al., 2016). Kahan et al. (2013) has demonstrated that hydration reaction of ketene can
64 form acetic acid under ambient conditions. Therefore, ketene has the potential to explain acetic
65 acid chemistry in the troposphere, notably near the biomass burning plumes (Akagi et al.,



66 2012;Yokelson et al., 2009). A recent theoretical study proposed that hydrolysis of ketene
67 produces acetic acid at a much faster rate in the atmosphere in presence of formic acid (Louie et
68 al., 2015). This mechanism pathway can facilitate hydrolysis of ketene if it is adsorbed into the
69 interface of SOA, and therefore can contribute to rapid growth of aerosols even in the absence of
70 a proper aqueous environment. A quantum chemical study recently showed that ammonolysis
71 (addition of NH_3) of ketene has the potential to produce acetamide (CH_3CONH_2) in the
72 troposphere (Sarkar et al., 2018). Photooxidation of this acetamide can produce isocyanic acid
73 (HNCO) that has potential health impacts such as cataracts, cardiovascular diseases, and
74 rheumatoid arthritis as it undergoes protein carbamylation (Wang et al., 2007;Roberts et al.,
75 2014;Sarkar et al., 2016).

76 In this study, we present evidence of direct emissions of ketene into the atmosphere from a
77 petrochemical facility in South Korea, detected by a high sensitivity proton transfer reaction time-
78 of-flight mass spectrometry (PTR-TOF-MS) technique during an aircraft measurement campaign
79 conducted in the summer (May-June) and fall (October) of 2019. Emission rate estimation of
80 ketene using a horizontal advective flux approach adapted from the top-down emission rate
81 retrieval algorithm (TERRA) (Gordon et al., 2015) with in-situ chemical and meteorological
82 observations is presented. Finally, an estimation of the OH reactivity and tropospheric O_3
83 production potential of ketene in the emission plumes is provided and their importance is discussed.

84 **2. Methods**

85 **2.1 Aircraft campaign**

86 Airborne VOC measurements were carried out during seven research flights of typically 3-4 hour
87 duration, conducted in the summer (May-June) and fall (October) of 2019, to characterize
88 emissions from large industrial facilities (coal power plants, steel mills and petrochemical facilities)
89 in the Taean Peninsula, located approximately 50 km south of Seoul metropolitan. A PTR-TOF-
90 MS (model 8000; Ionicon Analytic GmbH, Innsbruck, Austria) was deployed on the Hanseo
91 University research aircraft (Beechcraft 1900D, HL 5238) for VOC measurements along with a
92 fast-meteorological sensor (AIMMS 30; Aventech Research Inc.) that is capable of quantifying
93 aviation such as global positioning information, heading, angle of attack and meteorological data
94 such as water vapor, temperature, pressure, three dimensional wind field at 10 Hz resolution. To
95 capture real time emission activity, the research aircraft encircled individual industrial facilities at
96 a flight altitude of 300-1000 m above ground level. Table 1 provides details of the research flights
97 with VOC measurements during summer and fall aircraft campaigns while Figure 1 shows
98 locations of the industrial facilities and research flight tracks.

99 **2.2 VOC measurements**

100 VOC measurements were performed over major point and area sources (Daesan petrochemical
101 facility, Dangjin and Boryoung thermal power plants, Hyundai steel mills and Taean coal power



102 plants) using a high-sensitivity PTR-TOF-MS that enables high mass resolution with a detection
103 limit of low ppb to ppt using H_3O^+ as reagent ion (Lindinger et al., 1998; Jordan et al., 2009; Sarkar
104 et al., 2016; Sarkar et al., 2020). The PTR-TOF-MS was operated over the mass range of 21-210
105 amu at a drift tube pressure of 2.2 mbar and temperature of 60°C ($E/N \sim 136$ Td) that enabled
106 collection of VOC data at 1 Hz resolution. Ambient air was sampled continuously through a Teflon
107 inlet line (OD = 3/8"; length = 3 m) at an inlet flow rate of 100 sccm. To avoid any condensation
108 effect, inlet line was well insulated and heated to 40°C. Instrumental backgrounds were performed
109 using ambient air through a VOC scrubber catalyst heated to 350°C (GCU-s 0703, Ionimed
110 Analytik GmbH, Innsbruck, Austria).

111 The mixing ratio calculations for methanol, acetaldehyde, benzene and toluene reported in this
112 study were done by using the sensitivity factors (in ncps ppb^{-1}) obtained from the PTR-TOF-MS
113 calibrations performed using a gravimetric mixture of a 14-component VOC gas standard
114 ((Ionimed Analytik GmbH, Austria at ~ 1 ppm; stated accuracy better than 6% and NIST traceable)
115 containing methanol, acetonitrile, acetaldehyde, ethanol, acrolein, acetone, isoprene, methyl vinyl
116 ketone, methyl ethyl ketone, benzene, toluene, o-xylene, chlorobenzene, α -pinene and 1,2-
117 dichlorobenzene. Calibrations were performed in the range of 2-10 ppb. In order to establish the
118 instrumental background, VOC-free zero air was generated by passing the ambient air through a
119 catalytic converter (stainless steel tube filled with platinum-coated glass wool) heated at 350°C.
120 The measured ion signals were normalized to the primary ion (H_3O^+ , $m/z = 19$) as follows (Sarkar
121 et al., 2016; Sarkar et al., 2020):

$$122 \quad ncps = \frac{I(RH^+) \times 10^6}{I(H_3O^+)} \times \frac{2}{P_{drift}} \times \frac{T_{drift}}{298.15} \quad \dots (1)$$

123 The VOC sensitivities did not show any significant change during the calibrations performed as
124 the instrumental operating conditions remained constant, which is in agreement to several previous
125 studies (de Gouw and Warneke, 2007). Table S1 of the supplement lists the sensitivity factors for
126 methanol, acetaldehyde, benzene and toluene and their estimated limit of detection (LOD),
127 calculated as the 2σ value while measuring VOC free zero air at 1 Hz resolution (Sarkar et al.,
128 2016). VOCs for which we do not have any sensitivity factors from the calibrations (e. g. ketene),
129 concentrations were estimated based on the reaction rate constants as described by de Gouw and
130 Warneke (2007). A proton transfer reaction rate coefficient of $2.21 \times 10^{-9} \text{ cm}^3 \text{ s}^{-1}$ was used (Zhao
131 and Zhang, 2004) to calculate ketene concentrations. The estimated limit-of-detection (LOD) for
132 ketene was 0.58 ppb. Data acquisition and analysis of the PTR-TOF raw mass spectra was
133 accomplished using TofDaq (version 1.89; Tofwerk AG, Switzerland) and PTR-MS-viewer
134 (version 3.2; Ionicon Analytik GmbH, Innsbruck, Austria) softwares, respectively.

135

136



137 3. Results and Discussions

138 3.1 Detection of ketene using PTR-TOF-MS

139 For the identification of VOCs in the raw mass spectra, we followed the protocol described by
140 Sarkar et al. (2016) and attributed the ion peak detected at m/z 43.018 in the mass scan spectra to
141 monoisotopic mass of protonated ketene. Absence of any competing shoulder ion peaks between
142 42.968–43.068 amu (mass width bin of 0.05 amu) indicated no contribution from other ions in this
143 mass window as shown in Figure S1 of the supplement. The major advantage of using a PTR-
144 TOF-MS over a conventional PTR-Q-MS (with a quadrupole mass analyzer; Sarkar et al. (2013))
145 for VOC measurements is the ability of PTR-TOF-MS to separate the isobaric species such as
146 ketene (measured at m/z 43.018) and propene (measured at m/z 43.054) based on their
147 monoisotopic masses, allowing us to characterize more VOC species and thus minimize interfering
148 compounds. With the conventional PTR-Q-MS, both ketene and propene appear at a nominal mass
149 of m/z 43 and therefore, individual contribution of propene and ketene at m/z 43 remains unknown.
150 PTR-TOF-MS overcomes this limitation of PTR-Q-MS due to its high sensitivity and a mass
151 resolution of $m/\Delta m > 4000$, enabling separate detection of ketene (at m/z 43.018) and propene
152 (m/z 43.054). Detection of propene at m/z 43.054 using a PTR-TOF-MS is well established and
153 have been reported in several previous studies (Stockwell et al., 2015; Sarkar et al., 2016; Koss et
154 al., 2018). On the other hand, Ketene has been quantified only recently at m/z 43.018 using PTR-
155 TOF-MS in the ambient air (Jordan et al., 2009) and in laboratory biomass smoke (Stockwell et
156 al., 2015). Therefore, propene does not interfere in the detection of ketene using PTR-TOF-MS as
157 they show separate peaks in the raw mass spectra (Figure S2 of the supplement). Fragmentation
158 of propanol also results in propene which is detected at m/z 43.054 by PTR-TOF-MS and therefore,
159 propanol fragmentation does not interfere in the detection of ketene at m/z 43.018. Figure S3 of
160 the supplement shows the timeseries plot of the corrected ketene measured at $m/z = 43.018$ (in red)
161 and propene measured at $m/z = 43.054$ (in blue) during the research flight conducted on 29 May
162 morning. It can be seen from the timeseries that we detected propene as well in the emission plumes
163 from the petrochemical industries. A list of all the VOCs detected in the emission plumes from
164 petrochemical industries and other industrial facilities during our campaigns will be provided in a
165 companion paper (in preparation).

166 Accurate quantification of ketene with PTR-MS technique also depends on the fragmentation of
167 acetic acid (CH_3COOH) and glycolaldehyde ($\text{C}_2\text{H}_4\text{O}_2$) (Karl et al., 2007), parent ion of which is
168 measured at m/z 61.027 by PTR-TOF-MS (Stockwell et al., 2015; Sarkar et al., 2016). It is not
169 possible to differentiate structural isomers acetic acid and glycolaldehyde using PTR-TOF-MS,
170 however, $\sim 82\%$ of acetic acid is reported to contribute to the m/z 61.027 signal (Karl et al., 2007).
171 Fragmentation of this ion can significantly contribute to ketene signal ($m/z = 43.018$) in the mass
172 spectra. During our study, the measured ratio between m/z 61.027 and 43.018 outside of the peak
173 emission cases (Figure 2) was ~ 0.9 , which is consistent with the ratio reported in previous studies
174 at a similar E/N ratio (Hartungen et al., 2004; Haase et al., 2012). This indicates that the



175 fragmentation of acetic acid and glycolaldehyde results in about half at m/z 61.027 and the
176 remaining half at m/z 43.018, which is an interference for ketene signal and was subtracted to
177 obtain the corrected ketene concentrations. Henceforth, we refer to the m/z 43.018 signal, corrected
178 for the contribution of acetic acid and glycolaldehyde fragments, as ketene in this manuscript.

179 Figures 2a and 2b show timeseries plots for the mixing ratios of acetic acid and glycolaldehyde
180 parent ion ($m/z = 61.027$; in green), ketene fragment ($m/z = 43.018$; in brown) and the corrected
181 ketene (in red) during research flights conducted on 29 May morning and 1 June afternoon. It can
182 be seen from Figure 2a that there were several high peaks of ketene over the Daesan petrochemical
183 facility on 29 May. Such high peaks of ketene were observed over Daesan during all flights
184 conducted in the summer and fall (Figures 2b and S4 of the supplement). These high ketene peaks
185 are entirely absent in the timeseries of m/z 61.027, indicating that acetic acid and glycolaldehyde
186 fragmentation made a relatively small contribution to the signal detected in the emission plumes
187 over Daesan. Some peaks were also observed for both m/z 61.027 and m/z 43.018 over Dangjin
188 coal power plants and Hyundai steel mills during the flights conducted on 29 May and 23 October
189 (Figures 2a and S4 of the supplement). However, in most cases, these peaks of m/z 43.018
190 originated from the fragmentation of m/z 61.027, and so they do not contribute to the corrected
191 ketene signals. This further demonstrates that ketene has fresh emission sources in the plumes over
192 Daesan petrochemical facility. Since the measured ketene outside the plume was always < 2 ppb
193 (Figures 2 and S4 of the supplement), contribution from photochemically produced ketene would
194 be negligible, further indicating direct emission of ketene from the facility.

195 VOC correlation analyses were performed for the peak values to identify potential emission
196 sources for ketene at Daesan. Ketene showed strong correlations ($r^2 > 0.7$) with acetaldehyde,
197 methanol, benzene, and toluene, indicating commonality of emission sources. Figure S5 represents
198 example correlation plots between these VOCs during 28 October afternoon flight. Many of these
199 VOCs are emitted during high temperature production processes such as thermal cracking of
200 ethylene and production of polypropylene in the petrochemical industries (Cetin et al., 2003; Chen
201 et al., 2014; Mo et al., 2015). Daesan petrochemical facility is a major manufacturer of heat resistant
202 polypropylene in South Korea and therefore, ketene could potentially be produced during these
203 high temperature production processes. However, future studies focusing on VOC measurements
204 in the stacks and analysis using source apportionment models (e.g. USEPA-PMF; Sarkar et al.
205 (2017)) will improve our understanding of ketene emissions and chemistry at Daesan.

206 **3.2 Estimation of ketene emission rate using a horizontal advective flux approach**

207 Emission rates (ERs) of ketene and accompanying VOCs were estimated by integrating the
208 horizontal advective flux around Daesan petrochemical facility. A two-dimensional cylindrical
209 screen is created encompassing each facility during each flight. The mixing ratio flux through this
210 screen is then used to determine the emission rate coming from the interior of the screen. To create
211 the screen, a single horizontal path surrounding the facility is determined for flight tracks to



212 represent the horizontal component of the screen. The start of the horizontal path is approximately
213 set as the south-east corner of the ellipse and progresses in a counter-clockwise direction. The
214 horizontal path length (s) is calculated in meters and as a function of longitude (x) and latitude (y).
215 Each measurement point within 100 meters of the determined horizontal path is mapped to the
216 closest point on the horizontal path but retains its altitude (z). This creates a set of points on the
217 cylindrical screen. The measured mixing ratios of each compound, zonal wind (U), meridional
218 wind (V) and air density are interpolated to fill areas on the screen to a resolution of 40×20 meters
219 ($s \times z$). Interpolation is performed using a radial basis function with weights estimated by linear
220 least squares. The interpolated screens of zonal wind, meridional wind, and air density are used to
221 calculate the air flux ($E_{air,H}$) through the screen as follows:

$$222 \quad E_{air,H} = \iint \rho_{air} U_{\perp} ds dz \quad \dots (2)$$

223 Air density (ρ_{air}) is calculated at each flight position from the measured temperature (T), pressure
224 (p), and percent relative humidity (RH) as described by (Yau and Rogers, 1996):

$$225 \quad \rho_{air} = \frac{p}{RT(1 + 0.6\chi_{H_2O})}, \chi_{H_2O} = \frac{A_d \varepsilon}{p} \exp\left(\frac{T_d}{B_d}\right) \quad \dots (3)$$

226 where $R = 287.1 \text{ J kg}^{-1} \text{ K}^{-1}$; χ_{H_2O} is the water vapor mixing ratio; $A_d = 3.41 \times 10^9 \text{ kPa}$; $\varepsilon = 0.622$; B_d
227 $= 5420 \text{ K}$ and T_d is the dew-point temperature calculated using the August-Roche-Magnus
228 approximation as follows:

$$229 \quad T_d(T, RH) = \frac{\lambda \left(\ln\left(\frac{RH}{100}\right) + \frac{\beta T}{\lambda + T} \right)}{\beta - \left(\ln\left(\frac{RH}{100}\right) + \frac{\beta T}{\lambda + T} \right)} \quad \dots (4)$$

230 where $\lambda = 243.12^\circ\text{C}$ and $\beta = 17.62$.

231 The wind speed normal to the path is calculated as described by Gordon et al. (2015):

$$232 \quad U_{\perp} = \frac{V \frac{ds}{dx} - U \frac{ds}{dy}}{\sqrt{\left(\frac{ds}{dx}\right)^2 + \left(\frac{ds}{dy}\right)^2}} \quad \dots (5)$$

233 The mixing ratios of the compounds are interpolated for each point on the screen and combined
234 with the air flux to calculate the emission rate (ER) of the compounds using the following equation:

$$235 \quad ER = M_R \iint \chi_C \rho_{air} U_{\perp} ds dz \quad \dots (6)$$



236 where χ_C = mixing ratio of VOCs and M_R = ratio between compound molar mass and the molar
237 mass of air (42.04/28.97 for ketene). The air density (ρ_{air}) from the lowest flight track altitude is
238 approximated with a linear dependence on altitude. U_{\perp} is the normal wind vector (positive
239 outwards). Mixing ratios in the areas between the flight track measurements are interpolated using
240 a radial basis function with weights estimated by linear least square approximation. Interpolated
241 screens (resolution 40×20 m; horizontal \times altitude) of U, V wind and air density were then used
242 to retrieve air flux through the screens. This method is adapted from the TERRA approach
243 described by Gordon et al. (2015). The mass-balance approach was used to estimate emissions
244 through the top of the cylinder. Pressure and temperature were assumed to be constant during the
245 measurement timeframe. To determine emissions through the top of the cylinder, the following
246 mass-balance approach was used:

$$247 \quad E_{air,H} + E_{air,V} + E_{air,M} = 0 \quad \dots (7)$$

248 where, $E_{air,H}$ is the net horizontal air flux, $E_{air,V}$ is the net air flux through the top of the cylinder,
249 and $E_{air,M}$ is the change in air mass within the volume. We considered constant average pressure
250 and temperature for the duration of the observations to assume no change in air mass within the
251 volume. As a result, the air flux through the top of the cylinder can be considered $E_{air,V} = -E_{air,H}$.
252 The average value of the mixing ratio at the top of the cylinder is multiplied by $E_{air,V}$ to retrieve
253 emissions through the top of the cylinder.

254 Figures 3a and 3b depict mixing ratio screens for ketene for the 29 May morning and 28 October
255 afternoon flights. For both flights, highest ketene mixing ratios (χ_{ketene}) were measured near the
256 lowest flight path clearly indicating that surface emission sources caused the bulk of the ketene to
257 be below the flight track. The estimated net ERs (kg h^{-1}) for ketene and accompanying VOCs are
258 shown in Table 2a. The net ER represents emissions only from the facility and excludes the
259 contribution of emissions from outside sources that are upwind of the screen. The difference
260 between the estimated net ER and the ER going out of the screen (Table S2 of the supplement) for
261 ketene were $< 12\%$ for both flights. For 29 May flight, estimated net ketene ER was similar to that
262 of toluene and ~ 3 times lower than benzene while it was ~ 4 times lower than acetaldehyde. For
263 28 October flight, estimated net ketene ER was ~ 1.3 times lower and ~ 1.5 times higher than
264 benzene and toluene, respectively while it was ~ 2 times lower than acetaldehyde. These results
265 indicate that accurate estimation of ketene emissions from petrochemical facilities could be as
266 important as some of the major VOCs and therefore, including ketene (a rarely quantified VOC)
267 to the emission inventory will be a step forward towards effective VOC mitigation strategies.

268 To address the uncertainty in the extrapolation method below the measurement heights, we have
269 used two different approaches - **Approach 1**: we considered the nature of emissions from the
270 petrochemical facility being mainly from evaporative sources. As a result, we assumed that the
271 mixing ratios of ketene increases as it approaches the ground. This is observed when we used the
272 radial basis function to extrapolate linearly. To quantify the uncertainty in this extrapolation, we



273 assumed a constant value for heights under the measurement height equal to the mixing ratios at
274 the lowest observed altitude and defined it as a “constant” case. We assumed that the “constant”
275 case represents a lower end estimation due to the nature of the evaporative sources from the facility.
276 Then, we estimated the uncertainty due to ground extrapolation as the percentage change in
277 emission rates calculated from the linear radial basis function and from the “constant” case. The
278 estimated uncertainties were < 20% for most cases. For example, for the 29 May morning flight,
279 the estimated uncertainty was ~ 16% (Figure 4). As expected, this uncertainty is highly dependent
280 on the vertical position of the plume, with uncertainty being higher in cases where the highest
281 mixing ratio observed is at the lowest altitude measured. **Approach 2:** To assess the accuracy of
282 the radial basis function interpolation method, plumes resembling the observed plumes were
283 simulated. The plumes were generated based on a Gaussian distribution of the mixing ratio:

$$284 \quad \chi(s, z) = \sum_i \exp \left[-\frac{1}{2} \left(\left(\frac{s - s_{o,i}}{\sigma_{s,i}} \right)^2 + \left(\frac{z - z_{o,i}}{\sigma_{z,i}} \right)^2 \right) \right] \quad \dots (8)$$

285 where, χ is the mixing ratio, $s_{o,i}$ is the horizontal plume center, $z_{o,i}$ is the vertical plume center,
286 and i is the plume number. The parameters used for each date are listed in Table S3 of the
287 supplement. The flight path of each date is used to sample the simulated plume on the screen. The
288 simulated Gaussian plume is then reconstructed using the radial basis function interpolation based
289 on the points sampled from the simulated plume. Figure 5 shows the simulated plumes and radial
290 basis function-interpolated plumes for the 29 May and 28 October flights. The root-mean square
291 (RMS) and correlation coefficient (R^2) values were calculated to compare the simulated plume
292 with the radial basis function-interpolated plumes. The calculated RMS and R^2 values for 29 May
293 were 0.034 and 0.983, respectively. For 28 October, calculated RMS and R^2 values were 0.018
294 and 0.991, respectively.

295 **3.3 OH reactivity and O₃ production potential**

296 The OH reactivity of ketene was calculated according to the following equation (Sinha et al., 2012):

$$297 \quad \text{Ketene OH reactivity} = k_{\text{Ketene+OH}} [\text{Ketene}] \quad \dots (9)$$

298 where $k_{\text{Ketene+OH}}$ = first-order rate coefficient for the reaction of ketene with OH radicals and
299 $[\text{Ketene}]$ = measured mixing ratio of ketene. The rate coefficient of $3.38 \times 10^{-11} \text{ cm}^3 \text{ molecule}^{-1} \text{ s}^{-1}$
300 was used for the reaction of ketene with OH (Brown et al., 1989). For the 29 May and 1 June
301 flights (summer campaign), calculated average ketene OH reactivity for the emission plumes over
302 Daesan were 5.42 and 7.75 s^{-1} , respectively. The average OH reactivities during research flights
303 conducted in October (fall campaign) ranged from 3.33 to 7.35 s^{-1} . Table 2b shows the calculated
304 average and maximum OH reactivity and O₃ production potential of ketene during seven research
305 flights. Several previous studies have reported 50% or more missing OH reactivities near industrial
306 areas (Kim et al., 2011; Ryerson et al., 2003) and showed large uncertainties affecting HO_x budget.



307 Ambient ketene was not quantified in these studies due to absence of PTR-TOF-MS and the
308 attribution of nominal mass of m/z 43 (detected by PTR-QMS) only to propene. With PTR-TOF-
309 MS measurements, it is clear that both propene and ketene can contribute to the nominal mass of
310 m/z 43. While the rate coefficient of propene with OH radical is about 10% lower (3×10^{-11} and
311 $3.38 \times 10^{-11} \text{ cm}^3 \text{ molecule}^{-1} \text{ s}^{-1}$ for propene (Atkinson et al., 2006) and ketene (Brown et al., 1989),
312 respectively at 298 K), their chemical reactions with OH would be different since ketene contains
313 a carbonyl functional group ($\text{H}_2\text{C}=\text{C}=\text{O}$) but propene is an alkene ($\text{H}_3\text{C}-\text{C}=\text{CH}_2$). Therefore,
314 quantification of ketene will improve our estimation of the missing OH reactivity.

315 Tropospheric O_3 formation is significantly influenced by VOCs in polluted environments and has
316 strong impacts on air quality (ability to form photochemical smog), climate (contribution to
317 radiative forcing), human health (a pulmonary irritant) and can cause decreased crop yields
318 (Monks et al., 2015; Jerrett et al., 2009). The O_3 production potential of ketene was calculated
319 according to the following equation (Sinha et al., 2012):

$$320 \quad O_3 \text{ production potential} = (\text{Ketene OH reactivity}) \times [\text{OH}] \quad \dots (10)$$

321 Average OH radical concentration of $6.2 \times 10^6 \text{ molecules cm}^{-3}$, derived using a reactive plume
322 model considering NO_x photochemistry (with 255 condensed photochemical reactions) in power-
323 plant plumes (Kim et al., 2017), was used for the O_3 production potential calculation. The
324 calculated atmospheric lifetime of ketene using this OH concentration was ~ 1.4 h, indicating that
325 the spatial scale for which ketene would be effective in photochemistry could be at least a few km
326 (e. g. ~ 10 km assuming horizontal wind speed of 2 m s^{-1}). For the 29 May and 1 June flights,
327 calculated average O_3 production potential for ketene in the emission plumes over Daesan were
328 4.84 and 6.91 ppb h^{-1} , respectively. For research flights conducted in October (fall campaign),
329 average O_3 production potential ranged from 2.98 to 6.56 ppb h^{-1} (Table 2b). However, maximum
330 O_3 production potential for ketene at Daesan was 45.70 ppb h^{-1} on 1 June. Due to its fast reaction
331 rate with OH, ketene can contribute significantly to VOC OH reactivity, and hence O_3 production,
332 and a quantitative understanding of ketene is vital for tropospheric O_3 mitigation efforts. Therefore,
333 it is important to carry out further field and chamber studies to investigate the implications of
334 ketene photo-oxidation on HO_x chemistry and the atmospheric fate of ketene.

335 4. Conclusions

336 Ketene, a rare and highly reactive VOC, was identified and quantified using PTR-TOF-MS
337 technique in the emission plumes of Daesan petrochemical facility in South Korea during aircraft
338 measurement campaigns conducted in the summer (May-June) and Fall (October) of 2019. Ketene
339 mixing ratios of ~ 40 -50 ppb were measured in the emission plumes. Estimated ketene emission
340 rates from the facility using a horizontal advective flux approach ranged from 84-316 kg h^{-1} .
341 Ketene emission rates were compared to the estimated emission rates of benzene, toluene, and
342 acetaldehyde. In most cases, ketene emission rates were comparable to toluene. During peak
343 emissions, ketene also showed significant correlations ($r^2 > 0.7$) with acetaldehyde, methanol,



344 benzene, and toluene, indicating emissions of these VOCs occur from common processes. The
345 petrochemical facility at Daesan is the largest producer of heat resistant polypropylene in South
346 Korea and the high temperature production processes of polypropylene could be a potential source
347 of ketene at Daesan. However, future VOC measurement studies focusing on the stack emissions
348 at Daesan in combination with source apportionment models such as USEPA-PMF will provide
349 better insights on ketene emissions and chemistry at Daesan petrochemical facility.

350 For the emission plumes over Daesan, calculated average OH reactivity for ketene ranged from
351 3.33-7.75 s⁻¹. This indicates the importance of the quantification of ketene in the polluted
352 environment to address the puzzle of missing OH reactivity. During this study, calculated average
353 ketene O₃ production potential ranged from 2.98-6.91 ppb h⁻¹. Our study suggests that ketene can
354 potentially influence local photochemistry. Therefore, future studies focusing on the
355 photooxidation processes and atmospheric fate of ketene using chamber studies is required to get
356 a better insight of ketene formation in the atmosphere. Such studies will also improve our current
357 understanding of VOC-OH reactivity and hence secondary pollutants formation.

358

359

360 **Acknowledgements**

361 The authors thankfully acknowledge this research by the National Strategic Project-Fine Particle
362 of the National Research Foundation of Korea (NRF) funded by the Ministry of Science and ICT
363 (MSIT), the Ministry of Environment (ME), and the Ministry of Health and Welfare
364 (MOHW) (2019M3D8A1067406) and National Institute of Environmental Research (NIER-
365 RP2019-152) of South Korea for funding and logistical supports. We also appreciate helpful
366 discussion on the TERRA application generously provided by Andrea Darlington at
367 Environmental Canada and Mark Gordon at York University, Canada. S. K. would like to
368 acknowledge a funding support from Brain Pool Program of National Research Foundation Korea
369 (NRF) Funded by the Ministry of Science ICT (# 2020H1D3A2A01060699)

370 **Data Availability**

371 The observational data will be available upon the request to the corresponding authors.

372 **Author Contributions**

373 A. G., T. L., J. A., S. B. P., and S. K. conceptualized the study; C. S., G. W., A. M., T. P., J. B., S.
374 K., J-S. P., D. K., H. K., J. C., B-K. S., and J-H. K. conducted the field measurements; C. S., G.
375 W., S. K., and A. G. analyzed the data; A. G., T. L., J. A., S. B. P., and S. K. supervised the research
376 and administered the project; C. S., G. W., S. K., and A. G. wrote the original draft; All authors



377 reviewed and edited the manuscript; All authors have given approval to the final version of the
378 manuscript.

379 **Conflict of Interest Disclosure**

380 The authors declare no competing financial interest.

381 **References**

- 382 Akagi, S. K., Craven, J. S., Taylor, J. W., McMeeking, G. R., Yokelson, R. J., Burling, I. R.,
383 Urbanski, S. P., Wold, C. E., Seinfeld, J. H., Coe, H., Alvarado, M. J., and Weise, D. R.: Evolution
384 of trace gases and particles emitted by a chaparral fire in California, *Atmos. Chem. Phys.*, 12,
385 1397-1421, 10.5194/acp-12-1397-2012, 2012.
- 386 Atkinson, R.: Atmospheric chemistry of VOCs and NO_x, *Atmospheric Environment*, 34, 2063-
387 2101, [https://doi.org/10.1016/S1352-2310\(99\)00460-4](https://doi.org/10.1016/S1352-2310(99)00460-4), 2000.
- 388 Atkinson, R., Baulch, D. L., Cox, R. A., Crowley, J. N., Hampson, R. F., Hynes, R. G., Jenkin, M.
389 E., Rossi, M. J., Troe, J., and Subcommittee, I.: Evaluated kinetic and photochemical data for
390 atmospheric chemistry: Volume II – gas phase reactions of organic species, *Atmos. Chem.*
391 *Phys.*, 6, 3625-4055, 10.5194/acp-6-3625-2006, 2006.
- 392 Brown, A. C., Canosa-Mas, C. E., Parr, A. D., and Wayne, R. P.: Temperature dependence of the
393 rate of the reaction between the OH radical and ketene, *Chemical Physics Letters*, 161, 491-496,
394 [https://doi.org/10.1016/0009-2614\(89\)87026-5](https://doi.org/10.1016/0009-2614(89)87026-5), 1989.
- 395 Cetin, E., Odabasi, M., and Seyfioglu, R.: Ambient volatile organic compound (VOC)
396 concentrations around a petrochemical complex and a petroleum refinery, *Science of The Total*
397 *Environment*, 312, 103-112, [https://doi.org/10.1016/S0048-9697\(03\)00197-9](https://doi.org/10.1016/S0048-9697(03)00197-9), 2003.
- 398 Chen, M.-H., Yuan, C.-S., and Wang, L.-C.: Source Identification of VOCs in a Petrochemical
399 Complex by Applying Open-Path Fourier Transform Infrared Spectrometry, *Aerosol and Air*
400 *Quality Research*, 14, 1630-1638, 10.4209/aaqr.2014.04.0079, 2014.
- 401 de Gouw, J., and Warneke, C.: Measurements of volatile organic compounds in the earth's
402 atmosphere using proton-transfer-reaction mass spectrometry, *Mass Spectrometry Reviews*, 26,
403 223-257, 10.1002/mas.20119, 2007.
- 404 Gordon, M., Li, S. M., Staebler, R., Darlington, A., Hayden, K., O'Brien, J., and Wolde, M.:
405 Determining air pollutant emission rates based on mass balance using airborne measurement data
406 over the Alberta oil sands operations, *Atmos. Meas. Tech.*, 8, 3745-3765, 10.5194/amt-8-3745-
407 2015, 2015.
- 408 Haase, K. B., Keene, W. C., Pszenny, A. A. P., Mayne, H. R., Talbot, R. W., and Sive, B. C.:
409 Calibration and intercomparison of acetic acid measurements using proton-transfer-reaction mass
410 spectrometry (PTR-MS), *Atmos. Meas. Tech.*, 5, 2739-2750, 10.5194/amt-5-2739-2012, 2012.
- 411 Hartungen, E. v., Wisthaler, A., Mikoviny, T., Jaksch, D., Boscaini, E., Dunphy, P. J., and Märk,
412 T. D.: Proton-transfer-reaction mass spectrometry (PTR-MS) of carboxylic acids: Determination



413 of Henry's law constants and axillary odour investigations, *International Journal of Mass*
414 *Spectrometry*, 239, 243-248, <https://doi.org/10.1016/j.ijms.2004.09.009>, 2004.

415 IPCC: Impacts, Adaptation and Vulnerability: Working Group II: Contribution to the
416 Intergovernmental Panel on Climate Change: Fifth Assessment Report: Summary for
417 Policymakers, Intergovernmental Panel on Climate Change. Working Group Impacts, Cambridge
418 University Press, Cambridge, UK and New York, NY, USA, 1–32, 2013.

419 Jerrett, M., Burnett, R. T., Pope, C. A., Ito, K., Thurston, G., Krewski, D., Shi, Y., Calle, E., and
420 Thun, M.: Long-Term Ozone Exposure and Mortality, *New England Journal of Medicine*, 360,
421 1085-1095, [10.1056/NEJMoa0803894](https://doi.org/10.1056/NEJMoa0803894), 2009.

422 Jordan, A., Haidacher, S., Hanel, G., Hartungen, E., Märk, L., Seehauser, H., Schottkowsky, R.,
423 Sulzer, P., and Märk, T. D.: A high resolution and high sensitivity proton-transfer-reaction time-
424 of-flight mass spectrometer (PTR-TOF-MS), *International Journal of Mass Spectrometry*, 286,
425 122-128, <http://dx.doi.org/10.1016/j.ijms.2009.07.005>, 2009.

426 Kahan, T. F., Ormond, T. K., Ellison, G. B., and Vaida, V.: Acetic acid formation via the hydration
427 of gas-phase ketene under ambient conditions, *Chemical Physics Letters*, 565, 1-4,
428 <https://doi.org/10.1016/j.cplett.2013.02.030>, 2013.

429 Karl, T. G., Christian, T. J., Yokelson, R. J., Artaxo, P., Hao, W. M., and Guenther, A.: The
430 Tropical Forest and Fire Emissions Experiment: method evaluation of volatile organic compound
431 emissions measured by PTR-MS, FTIR, and GC from tropical biomass burning, *Atmos. Chem.*
432 *Phys.*, 7, 5883-5897, [10.5194/acp-7-5883-2007](https://doi.org/10.5194/acp-7-5883-2007), 2007.

433 Kim, S. W., McKeen, S. A., Frost, G. J., Lee, S. H., Trainer, M., Richter, A., Angevine, W. M.,
434 Atlas, E., Bianco, L., Boersma, K. F., Brioude, J., Burrows, J. P., de Gouw, J., Fried, A., Gleason,
435 J., Hilboll, A., Mellqvist, J., Peischl, J., Richter, D., Rivera, C., Ryerson, T., te Lintel Hekkert, S.,
436 Walega, J., Warneke, C., Weibring, P., and Williams, E.: Evaluations of NO_x and highly reactive
437 VOC emission inventories in Texas and their implications for ozone plume simulations during the
438 Texas Air Quality Study 2006, *Atmos. Chem. Phys.*, 11, 11361-11386, [10.5194/acp-11-11361-](https://doi.org/10.5194/acp-11-11361-2011)
439 2011, 2011.

440 Kim, Y. H., Kim, H. S., and Song, C. H.: Development of a Reactive Plume Model for the
441 Consideration of Power-Plant Plume Photochemistry and Its Applications, *Environmental Science*
442 *& Technology*, 51, 1477-1487, [10.1021/acs.est.6b03919](https://doi.org/10.1021/acs.est.6b03919), 2017.

443 Klotz, B., Barnes, I., H. Becker, K., and T. Golding, B.: Atmospheric chemistry of benzene
444 oxide/oxepin, *Journal of the Chemical Society, Faraday Transactions*, 93, 1507-1516,
445 [10.1039/A606152D](https://doi.org/10.1039/A606152D), 1997.

446 Koss, A. R., Sekimoto, K., Gilman, J. B., Selimovic, V., Coggon, M. M., Zarzana, K. J., Yuan, B.,
447 Lerner, B. M., Brown, S. S., Jimenez, J. L., Krechmer, J., Roberts, J. M., Warneke, C., Yokelson,
448 R. J., and de Gouw, J.: Non-methane organic gas emissions from biomass burning: identification,
449 quantification, and emission factors from PTR-ToF during the FIREX 2016 laboratory experiment,
450 *Atmos. Chem. Phys.*, 18, 3299-3319, [10.5194/acp-18-3299-2018](https://doi.org/10.5194/acp-18-3299-2018), 2018.



- 451 Lelieveld, J., Dentener, F. J., Peters, W., and Krol, M. C.: On the role of hydroxyl radicals in the
452 self-cleansing capacity of the troposphere, *Atmos. Chem. Phys.*, 4, 2337-2344, 10.5194/acp-4-
453 2337-2004, 2004.
- 454 Lelieveld, J., Gromov, S., Pozzer, A., and Taraborrelli, D.: Global tropospheric hydroxyl
455 distribution, budget and reactivity, *Atmos. Chem. Phys.*, 16, 12477-12493, 10.5194/acp-16-12477-
456 2016, 2016.
- 457 Lindinger, W., Hansel, A., and Jordan, A.: On-line monitoring of volatile organic compounds at
458 pptv levels by means of proton-transfer-reaction mass spectrometry (PTR-MS) medical
459 applications, food control and environmental research, *International Journal of Mass Spectrometry
460 and Ion Processes*, 173, 191-241, [https://doi.org/10.1016/S0168-1176\(97\)00281-4](https://doi.org/10.1016/S0168-1176(97)00281-4), 1998.
- 461 Louie, M. K., Francisco, J. S., Verdicchio, M., Klippenstein, S. J., and Sinha, A.: Hydrolysis of
462 Ketene Catalyzed by Formic Acid: Modification of Reaction Mechanism, Energetics, and Kinetics
463 with Organic Acid Catalysis, *The Journal of Physical Chemistry A*, 119, 4347-4357,
464 10.1021/jp5076725, 2015.
- 465 McNelis, D. N., Ripperton, L., Wilson, W. E., Hanst, P. L., and Gay, B. W.: Gas-Phase Reactions
466 of Ozone and Olefin in the Presence of Sulfur Dioxide, in: *Removal of Trace Contaminants from
467 the Air*, ACS Symposium Series, 17, American Chemical Society, 187-200, 1975.
- 468 Mo, Z., Shao, M., Lu, S., Qu, H., Zhou, M., Sun, J., and Gou, B.: Process-specific emission
469 characteristics of volatile organic compounds (VOCs) from petrochemical facilities in the Yangtze
470 River Delta, China, *Science of The Total Environment*, 533, 422-431,
471 <https://doi.org/10.1016/j.scitotenv.2015.06.089>, 2015.
- 472 Monks, P. S., Archibald, A. T., Colette, A., Cooper, O., Coyle, M., Derwent, R., Fowler, D.,
473 Granier, C., Law, K. S., Mills, G. E., Stevenson, D. S., Tarasova, O., Thouret, V., von
474 Schneidmesser, E., Sommariva, R., Wild, O., and Williams, M. L.: Tropospheric ozone and its
475 precursors from the urban to the global scale from air quality to short-lived climate forcer, *Atmos.
476 Chem. Phys.*, 15, 8889-8973, 10.5194/acp-15-8889-2015, 2015.
- 477 Roberts, J. M., Veres, P. R., VandenBoer, T. C., Warneke, C., Graus, M., Williams, E. J., Lefer,
478 B., Brock, C. A., Bahreini, R., Öztürk, F., Middlebrook, A. M., Wagner, N. L., Dubé, W. P., and
479 de Gouw, J. A.: New insights into atmospheric sources and sinks of isocyanic acid, HNCO, from
480 recent urban and regional observations, *Journal of Geophysical Research: Atmospheres*, 119,
481 1060-1072, 10.1002/2013jd019931, 2014.
- 482 Ryerson, T. B., Trainer, M., Angevine, W. M., Brock, C. A., Dissly, R. W., Fehsenfeld, F. C.,
483 Frost, G. J., Goldan, P. D., Holloway, J. S., Hübler, G., Jakoubek, R. O., Kuster, W. C., Neuman,
484 J. A., Nicks Jr., D. K., Parrish, D. D., Roberts, J. M., Sueper, D. T., Atlas, E. L., Donnelly, S. G.,
485 Flocke, F., Fried, A., Potter, W. T., Schaubler, S., Stroud, V., Weinheimer, A. J., Wert, B. P.,
486 Wiedinmyer, C., Alvarez, R. J., Banta, R. M., Darby, L. S., and Senff, C. J.: Effect of
487 petrochemical industrial emissions of reactive alkenes and NO_x on tropospheric ozone formation
488 in Houston, Texas, *Journal of Geophysical Research: Atmospheres*, 108, 10.1029/2002jd003070,
489 2003.



- 490 Sarkar, C., Kumar, V., and Sinha, V.: Massive emissions of carcinogenic benzenoids from paddy
491 residue burning in North India, *Current Science*, 104, 1703 - 1709, 2013.
- 492 Sarkar, C., Sinha, V., Kumar, V., Rupakheti, M., Panday, A., Mahata, K. S., Rupakheti, D.,
493 Kathayat, B., and Lawrence, M. G.: Overview of VOC emissions and chemistry from PTR-TOF-
494 MS measurements during the SusKat-ABC campaign: high acetaldehyde, isoprene and isocyanic
495 acid in wintertime air of the Kathmandu Valley, *Atmos. Chem. Phys.*, 16, 3979-4003, 10.5194/acp-
496 16-3979-2016, 2016.
- 497 Sarkar, C., Sinha, V., Sinha, B., Panday, A. K., Rupakheti, M., and Lawrence, M. G.: Source
498 apportionment of NMVOCs in the Kathmandu Valley during the SusKat-ABC international field
499 campaign using positive matrix factorization, *Atmos. Chem. Phys.*, 17, 8129-8156, 10.5194/acp-
500 17-8129-2017, 2017.
- 501 Sarkar, C., Guenther, A. B., Park, J. H., Seco, R., Alves, E., Batalha, S., Santana, R., Kim, S.,
502 Smith, J., Tóta, J., and Vega, O.: PTR-TOF-MS eddy covariance measurements of isoprene and
503 monoterpene fluxes from an eastern Amazonian rainforest, *Atmos. Chem. Phys.*, 20, 7179-7191,
504 10.5194/acp-20-7179-2020, 2020.
- 505 Sarkar, S., Mallick, S., Kumar, P., and Bandyopadhyay, B.: Ammonolysis of ketene as a potential
506 source of acetamide in the troposphere: a quantum chemical investigation, *Physical Chemistry
507 Chemical Physics*, 20, 13437-13447, 10.1039/C8CP01650J, 2018.
- 508 Sinha, V., Williams, J., Diesch, J. M., Drewnick, F., Martinez, M., Harder, H., Regelin, E.,
509 Kubistin, D., Bozem, H., Hosaynali-Beygi, Z., Fischer, H., Andrés-Hernández, M. D., Kartal, D.,
510 Adame, J. A., and Lelieveld, J.: Constraints on instantaneous ozone production rates and regimes
511 during DOMINO derived using in-situ OH reactivity measurements, *Atmos. Chem. Phys.*, 12,
512 7269-7283, 10.5194/acp-12-7269-2012, 2012.
- 513 Stockwell, C. E., Veres, P. R., Williams, J., and Yokelson, R. J.: Characterization of biomass
514 burning emissions from cooking fires, peat, crop residue, and other fuels with high-resolution
515 proton-transfer-reaction time-of-flight mass spectrometry, *Atmos. Chem. Phys.*, 15, 845-865,
516 10.5194/acp-15-845-2015, 2015.
- 517 Wang, Z., Nicholls, S. J., Rodriguez, E. R., Kumm, O., Hörkkö, S., Barnard, J., Reynolds, W. F.,
518 Topol, E. J., DiDonato, J. A., and Hazen, S. L.: Protein carbamylation links inflammation,
519 smoking, uremia and atherogenesis, *Nature medicine*, 13, 1176-1184, 10.1038/nm1637, 2007.
- 520 Wu, D., and O'Shea, D. F.: Potential for release of pulmonary toxic ketene from vaping pyrolysis
521 of vitamin E acetate, *Proceedings of the National Academy of Sciences*, 117, 6349-6355,
522 10.1073/pnas.1920925117, 2020.
- 523 Yau, M. K. a., and Rogers, R. R.: *A Short Course in Cloud Physics*, Elsevier Science, Saint Louis,
524 3rd Edition,, 1996.
- 525 Yokelson, R. J., Crounse, J. D., DeCarlo, P. F., Karl, T., Urbanski, S., Atlas, E., Campos, T.,
526 Shinozuka, Y., Kapustin, V., Clarke, A. D., Weinheimer, A., Knapp, D. J., Montzka, D. D.,
527 Holloway, J., Weibring, P., Flocke, F., Zheng, W., Toohey, D., Wennberg, P. O., Wiedinmyer, C.,
528 Mauldin, L., Fried, A., Richter, D., Walega, J., Jimenez, J. L., Adachi, K., Buseck, P. R., Hall, S.



529 R., and Shetter, R.: Emissions from biomass burning in the Yucatan, Atmos. Chem. Phys., 9, 5785-
 530 5812, 10.5194/acp-9-5785-2009, 2009.

531 Zhao, J., and Zhang, R.: Proton transfer reaction rate constants between hydronium ion (H₃O⁺)
 532 and volatile organic compounds, Atmospheric Environment, 38, 2177-2185,
 533 https://doi.org/10.1016/j.atmosenv.2004.01.019, 2004.

534

535

536

537 **Table 1.** Summary of research flights with VOC measurements during the summer (May-June)
 538 and fall (October) aircraft campaigns in South Korea

Date	Flight No.	Start Time (LT)	End Time (LT)	Facilities Included	Flight Design	Wind Direction
Summer 2019:						
29 May	1	09:32	12:36	Daesan, Dangjin, Hyundai	Circular spirals at 6 altitudes; 300 - 1100 m	Southwest
1 June	2	13:42	16:13	Boryoung, Daesan, Dangjin, Hyundai	Circular spirals at 6 altitudes; 300 - 1100 m	Wind data not available
Fall 2019:						
23 October	3	13:30	16:45	Boryoung, Taean, Daesan, Dangjin, Hyundai	Racetrack and circular spirals at a single altitude ~ 400 m	East
28 October	4	13:38	16:48	Daesan, Hyundai	Racetrack spirals and crosstrack at 2 altitudes; 400 - 600 m	Southwest
29 October	5	08:14	11:14	Daesan, Hyundai	Racetrack and circular spirals at 2 altitudes; 400 - 600 m	West
30 October	6	13:32	16:48	Boryoung, Taean, Daesan, Dangjin, Hyundai	Racetrack and circular spirals at	West



					3 altitudes; 400 - 1000 m
31 October	7	13:33	15:34	Boryung, Taean, Daesan, Dangjin, Hyundai	Racetrack and Wind data circular spirals at not available 3 altitudes; 400 - 1000 m

539

540

541

542 **Table 2.** a) Net emission rates (kg h^{-1}) of ketene, benzene, acetaldehyde and toluene over Daesan
 543 petrochemical facility; b) calculated OH reactivity (s^{-1}) and O_3 production potential (ppb h^{-1}) of
 544 ketene during emission plumes measured over Daesan petrochemical facility

a) Research Flights	Ketene (kg h^{-1})	Benzene (kg h^{-1})	Acetaldehyde (kg h^{-1})	Toluene (kg h^{-1})
<u>Summer 2019:</u>				
29 May Morning	312	917	1256	314
<u>Fall 2019:</u>				
23 October Afternoon	286	146	-1	-43
28 October Afternoon	316	426	619	210
29 October Morning	27	241	430	103
30 October Afternoon	84	211	359	102
b) Research Flights	OH reactivity (s^{-1})*		O_3 production potential (ppb h^{-1})*	
<u>Summer 2019:</u>				
29 May Morning	5.42 (33.76)		4.84 (30.10)	
1 June Afternoon	7.75 (51.24)		6.91 (45.70)	
<u>Fall 2019:</u>				
23 October Afternoon	7.35 (33.33)		6.56 (29.80)	
28 October Afternoon	5.28 (15.74)		4.71 (14.00)	
29 October Morning	3.79 (14.77)		3.38 (13.20)	
30 October Afternoon	3.33 (19.71)		2.98 (17.60)	
31 October Afternoon	4.56 (8.09)		4.07 (7.22)	

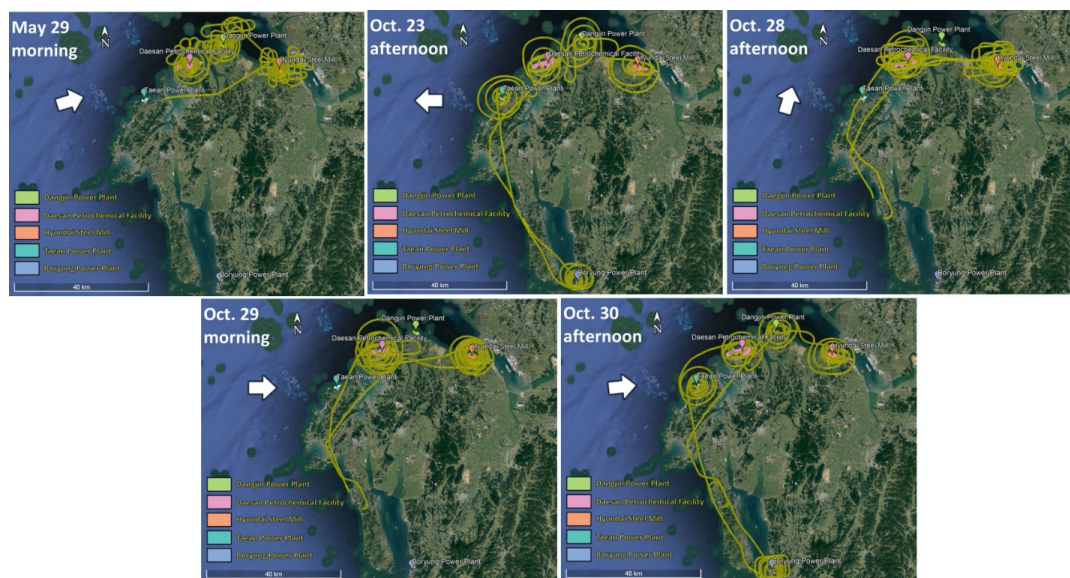
545 *Values in the parentheses represents maximum OH reactivity and O_3 production potential

546

547

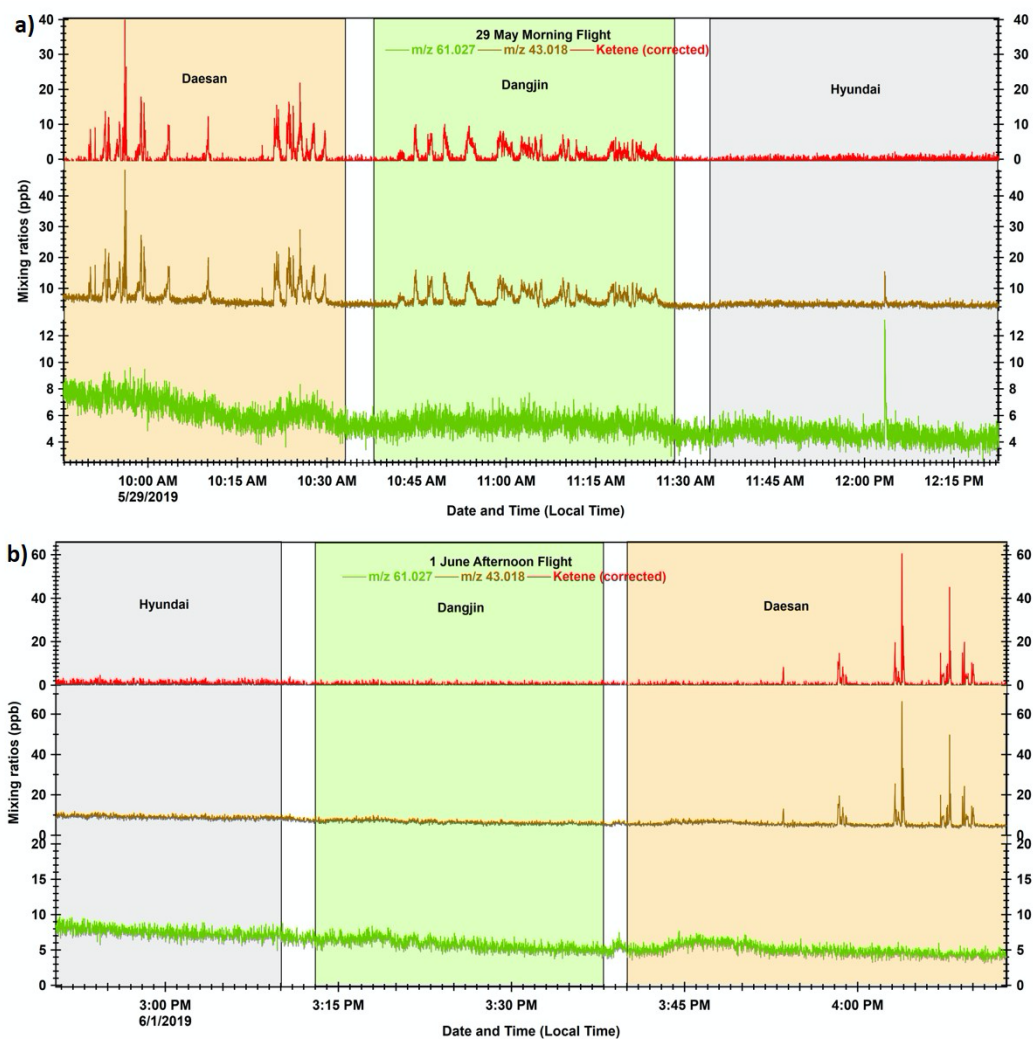


548
549
550
551
552
553
554



555
556
557
558
559
560
561
562
563

Figure 1. Composite ©Google Earth images showing research flight tracks over the Daesan petrochemical facility, Dangjin and Boryoung thermal power plants, Hyundai steel mills and Taean coal power plants during the airborne study conducted in summer (May-June 2019) and fall (October 2019). The white arrow in each plot represents mean wind direction during the flight. Only those flights are shown for which wind direction measurements were available



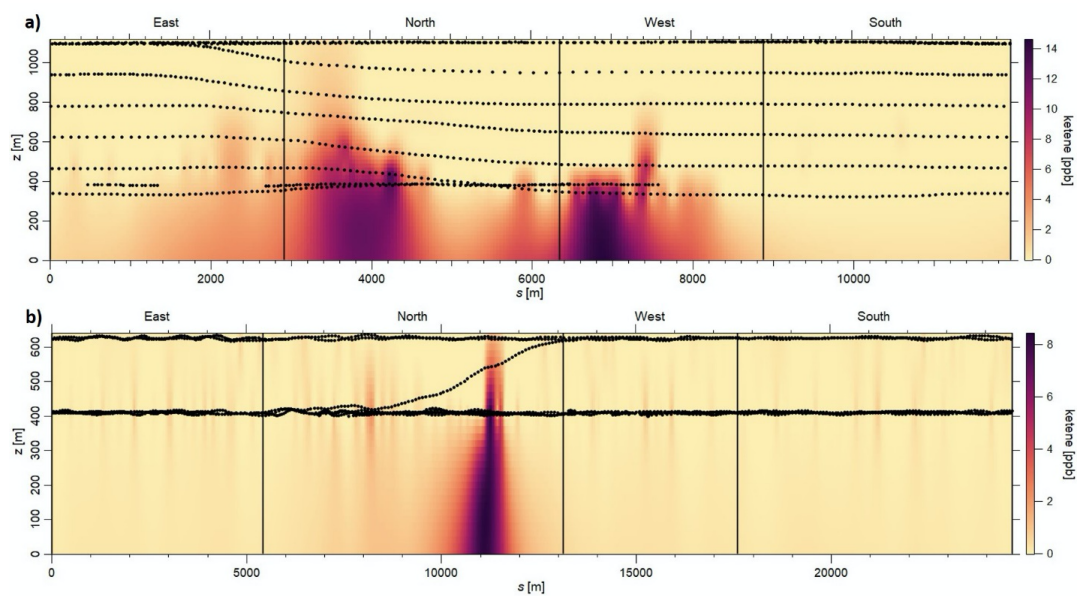
571

572 **Figure 2.** Timeseries profiles for mixing ratios (1 Hz resolution) of acetic acid and glycolaldehyde
573 parent ion ($m/z = 61.027$), ketene fragment ($m/z = 43.018$) and corrected ketene (corrected for m/z
574 61.027 fragmentation) during a) 29 May morning flight and b) 1 June afternoon flight. The light
575 pink, light green and light blue shaded areas represent the duration for which the flights were flying
576 over Daesan, Dangjin and Hyundai, respectively

577

578

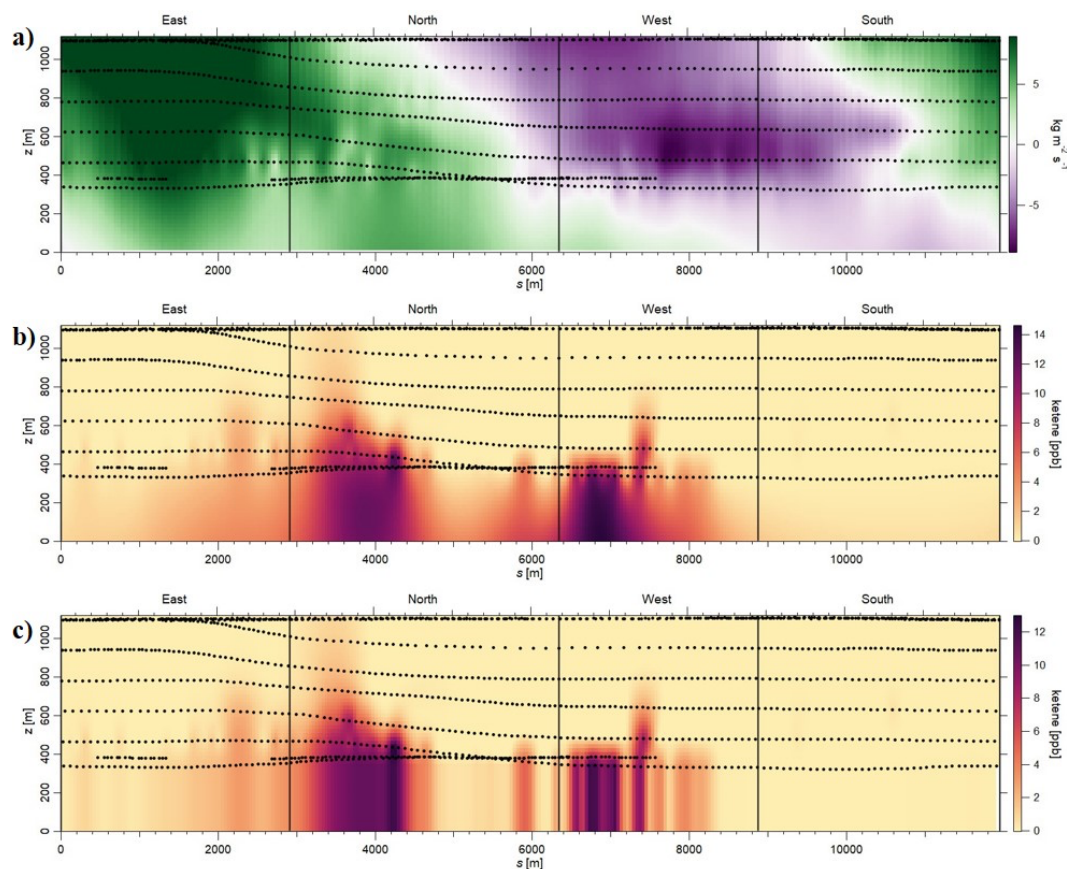
579



580

581 **Figure 3.** Kriging-interpolated ketene mixing ratios for a) 29 May morning and b) 28 October
582 afternoon flights. Black dots represent the flight path.

583



584

585 **Figure 4.** Estimation of uncertainty in the emission rates using approach 1 during 29 May morning
586 flight: a) Air flux screen (green = going out of the facility; purple = into the facility); b) Case 1:
587 Linear extrapolation using radial basis function (net emission rate from the facility = 312.36 kg h⁻¹;
588 emission rate going out of the screen = 357.73 kg h⁻¹); c) Case 2: Linear extrapolation using the
589 “constant case” (net emission rate from the facility = 262.44 kg h⁻¹; emission rate going out of the
590 screen = 298.74 kg h⁻¹; exponentials are the same for both the cases; uncertainty ~ 15.5% - 16%)

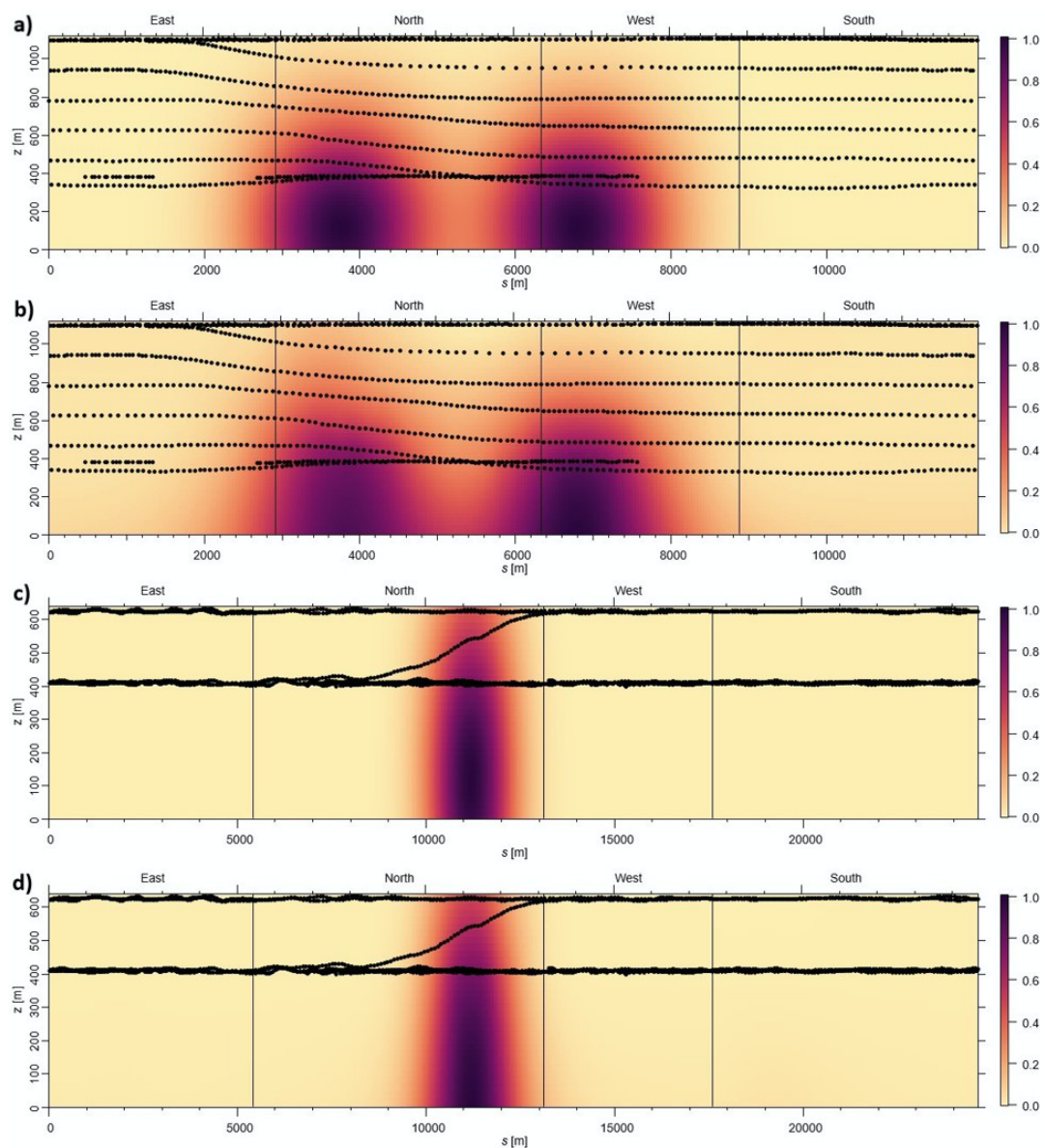
591

592

593

594

595



596

597 **Figure 5.** a) Simulated plume scenario and b) radial basis function-interpolated plume for May 29
598 morning flight. c) Simulated plume scenario and d) radial basis function-interpolated plume for
599 October 28 afternoon flight. Black dots are the flight position measurements of each flight.

600

601